

An innovative BRB with viscoelastic layers: performance evaluation and numerical simulation

Ying Zhou^{*}, Shunming Gong, Qing Hu and Rili Wu

State Key Laboratory of Disaster Reduction in Civil Engineering, Tongji University, Shanghai 20092, China

(Received November 2, 2017, Revised November 21, 2017, Accepted November 24, 2017)

Abstract. Energy induced by minor earthquake and micro vibration cannot be dissipated by traditional buckling-restrained braces (BRBs). To solve this problem, a new type of hybrid passive control device, named as VE-BRB, which is configured by a BRB with high-damping viscoelastic (VE) layers, is developed and studied. Theoretical analysis, performance tests, numerical simulation and case analysis are conducted to study the seismic behavior of VE-BRBs. The results indicate that the combination of hysteretic and damping devices lead to a multi-phased nature and good performance. VE-BRB's working state can be divided into three phases: before yielding of the steel core, VE layers provide sufficient damping ratio to mitigate minor vibrations; after yielding of the steel core, the steel's hysteretic deformations provide supplemental dissipative capacity for structures; after rupture of the steel core, VE layers are still able to work normally and provide multiple security assurance for structures. The simulation results agreed well with the experimental results, validating the finite element analysis method, constitutive models and the identified parameters. The comparison of the time history analysis on a 6-story frame with VE-BRBs and BRBs verified the advantages of VE-BRB for seismic protection of structures compared with traditional BRB. In general, VE-BRB had the potential to provide better control effect on structural displacement and shear in all stages than BRB as expected.

Keywords: buckling-restrained brace; viscoelastic material; hybrid passive control device; cyclic loading test; numerical simulation; time history analysis

1. Introduction

Moment resisting frames have been commonly used as building structural systems, which rely on the columns to provide lateral load resistance under earthquake actions. Due to columns' low lateral stiffness, however, their lateral displacements are generally large. This results in inelastic deformations under an earthquake, permanent structural damages which are beyond repair afterward, and possibly high cost for reconstructions and repairs. An alternative design approach is to concentrate the damage on sacrificial and easy to repair/replace members regarded as "structural fuses", which can dissipate the energy during earthquakes and preserve the safety of the main structure (Zhou *et al.* 2017, Zhou and Chen 2017, Gong and Zhou 2017, Zhou *et al.* 2012). The buckling-restrained brace (BRB) is one type of implementation of the structural fuse concept in current structures (Vargas and Bruneau 2009, El-Bahey and Bruneau 2010).

^{*}Corresponding author, Professor, E-mail: yingzhou@tongji.edu.cn

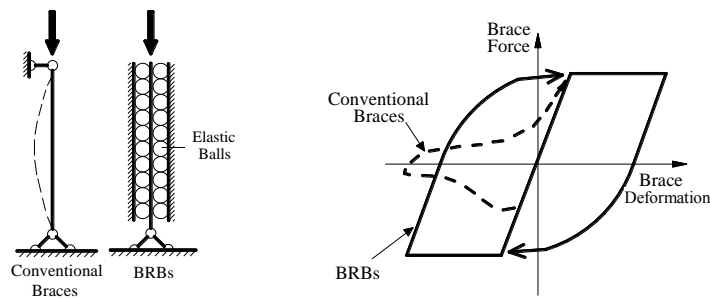


Fig. 1 Working principle of BRBs

A BRB consists of a load-carrying steel element, named as steel core, like a conventional brace and a lateral-support system. The lateral-support mechanism provides continuous lateral restraint to the steel core to prevent the brace from buckling when it is loaded under high compression forces. Consequently, its hysteresis loops are full and stable, and the behaviors under conditions of compression and tension are similar, which means that the device is very effective in dissipating seismic energy and will reduce the structural response. The mechanical working principle of a BRB compared to conventional braces can be seen in Fig. 1. Guneyisi (2012) and Mahrenholtz *et al.* (2015) studied the application and benefit of BRBs to steel structures and reinforced concrete (RC) structures, respectively. The results indicated that both for steel and RC structures, BRBs could improve significantly the seismic behavior and mitigate the structural response of the original buildings. Bazaez and Dusicka (2016), Wei and Bruneau (2016) also validated the control effectiveness of BRBs for RC bridge bents.

The effectiveness of BRBs used as hysteretic dampers to mitigate the response and improve the performance of structures during earthquakes has been well verified by both experimental and analytical research. Lee *et al.* (2013) conducted shaking table tests on a 1:5 scaled RC low-rise building model strengthened with BRBs at ground story, in which great enhancement in earthquake resistance was achieved. Khoo *et al.* (2016) carried out substructure pseudo-dynamic tests of a full-scale two-story frame with BRBs under bidirectional in-plane and out-of-plane loading. Di Sarno and Manfredi (2012) conducted experimental tests, using displacement-controlled pushover static and cyclic lateral loads, on a full-scale RC 2-storey 2-bays unretrofitted frame and a retrofitted one with BRBs. The results indicated that BRBs were effective devices to upgrade the lateral stiffness and strength of the RC frame buildings. Apostolakis and Dargush (2010) proposed a computational framework for the optimal distribution and design of BRBs installed in steel moment-resisting frames for a given seismic loading, in which a Genetic Algorithm was used to solve the resulting discrete optimization problem.

Although many studies have pointed out the remarkable ductility and control effect of BRBs, a small body of study exists on the improvement of the performance and applicability of BRBs. Previously developed upgraded BRBs made efforts mainly on the use of new materials and configurations. Usami *et al.* (2012) improved the BRB by using high-performance aluminum alloy instead of conventional low yield point steel, in order to enhance its durability for withstanding severe earthquakes three times without being replaced. Zhao *et al.* (2011) proposed an angle steel BRB (ABRB), in which four steel angles were used to form a non-welded cruciform shape steel core, and two external steel angles to form an external tube, to lead to an easier engineering application. Chou *et al.* (2016) studied a novel dual-core self-centering sandwiched BRB

(SC-SBRB) which was beneficial to develop a structural system having both energy dissipation and self-centering properties in earthquakes. Lin *et al.* (2016) investigated a thin-profile BRB (thin-BRB) which would reduce the width of the member and thus save usable space in buildings. Bozkurt and Topkaya (2016) developed a welded overlap core steel encased BRB to improve the cyclic performance. Zhang *et al.* (2016) studied an innovate type of BRB consisting of three steel tubes with slotted holes in the middle tube, test results indicated the BRB exhibited excellent deformation capacity and low-cycle fatigue behavior under appropriate opening-hole ratio and arrangement of the slotted holes on the middle tube.

However, all the improved BRBs mentioned above are of displacement-dependent device just like traditional BRB. Even in energy-dissipating states, these devices also provide great supplemental stiffness, resulting in an increase in the seismic effect to structures. Nevertheless, their metallic yielding core working as load-carrying element is usually designed to provide initial stiffness without energy dissipation under minor excitation until yielding under greater excitation. So it is necessary to introduce an extra velocity-dependent dissipation mechanism, such as viscous or viscoelastic types, which can effectively increase the additional damping ratio of the structure without significant added stiffness for all magnitudes of seismic loading. This is particularly important under minor vibrations, as input energy and dynamic response of structures will reduce, then the cross sections and material cost of the structural elements will decrease. Therefore, the combination of those two different dissipation mechanism minimizes the problems of individual dampers, and is a more economical solution for seismic mitigation (Marshall and Charney 2012). To implement this strategy, one common way in engineering application is to use two or more different types of dampers in a building at the same time. However, the combination use of multi-type dampers requires more arrangement locations and adversely affect architectural features and aesthetics.

To solve these problems, a new type of hybrid passive control device named as viscoelastic buckling-restrained brace (VE-BRB), which is configured as a BRB with high-damping viscoelastic (VE) layers, is developed in this study. The VE-BRB benefits from two types, namely hysteretic and damping dissipation mechanism at the same time in one assembled brace, which is a way having the least impact on the architectural appearance. Stiffness and dissipation capacity of VE-BRB are stronger than conventional BRB and VE damper due to the combination of both components to work together. VE-BRB has the potential to protect the structures over a broad range of earthquake magnitudes (displacement amplitudes), especially to reduce the construction cost based on structural design under minor earthquake and meet the comfort requirements under wind-induced vibrations. Fatigue capacity of high damping rubber is greater than low yield point steel, and therefore, even if the steel core is snapped under cyclic loading, the VE layers are still able to work normally and, thus, provide multiple security assurance for structures. Therefore, VE-BRB can be designed as part of a seismic protection system to meet multiple constraint performance-based specifications. The VE-BRB is investigated experimentally and analytically in this paper, the results obtained show that it features multi-phased nature and good performance, and its numerical simulation and case analysis are conducted to promote its application in engineering practice.

2. Concept of BRB

The typical configuration of a conventional BRB is shown in Fig. 2. The mild steel core of a

BRB works as a load-carrying and yielding component that resists the axial forces and dissipates the seismic energy input to the structure, and thus, withstand the expected ground motion. In order to prevent the steel core from buckling and have a balanced hysteresis behavior of the brace, the core is encased with a steel tube. In addition, between the steel core and the outer steel tube, there is mortar or concrete filling up the space to provide lateral support for steel core; this constitutes the restraining mechanism of a BRB. There is de-bonding material layer between the steel core and the concrete-filled steel tube (CFST) to avoid the friction effect and stress transfer. A cross section of a typical BRB and longitudinal segments of the steel core of conventional BRB are shown in Figs. 3 and 4, respectively.

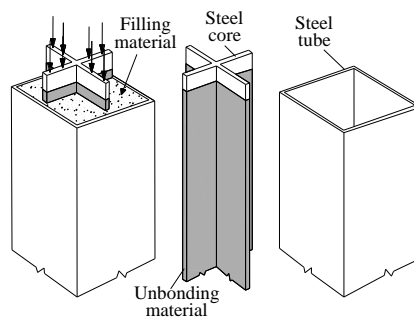


Fig. 2 Typical configuration of a BRB

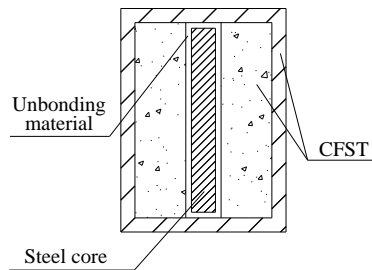


Fig. 3 Cross section of a BRB

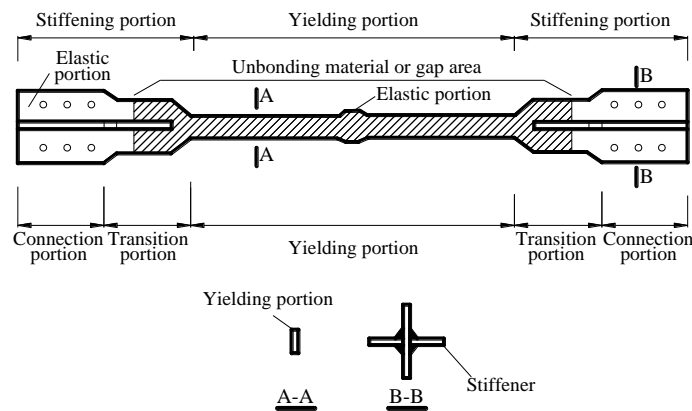


Fig. 4 Longitudinal construction segments of the steel core

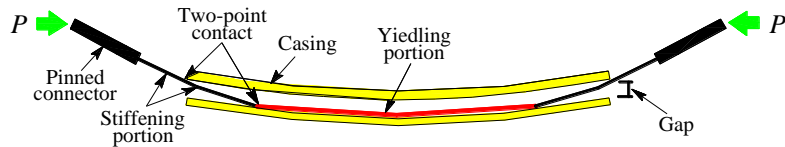


Fig. 5 Contact and forces transfer between the steel core and casing

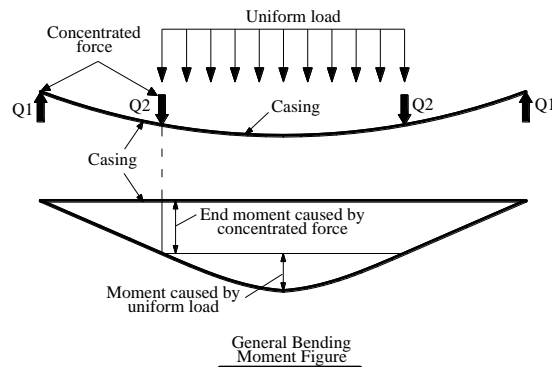


Fig. 6 Mechanical analysis and general moment diagram of the casing

As most types of passively controlled structures, the BRB-controlled structures use displacement between brace’s attachment points to generate axial deformations, controlling forces and energy dissipation. Under conditions of compression, the steel core tends to buckle before developing to its full capacity, but the casing can suppress the tendency of buckling for steel core. Both components of BRB contact each other (Poisson’s effect) and transfer forces as illustrated in Fig. 5. The casing mainly carries the moment and shear transferred from steel core as shown in Fig. 6. Therefore, the casing of BRB works mainly as a flexural member.

3. Proposal of VE-BRB

The control effect of conventional BRBs is not significant under small vibrations, caused by frequent earthquakes or strong winds, because they just provide additional stiffness but no additional damping to a structure during small vibrations. To ensure the comfort levels for the occupants of a building, especially in the case of tall buildings, vibration control capacity during frequent earthquakes and strong winds is also required. Thus, the concept of VE-BRB is proposed to meet this requirement; the VE-BRB can be defined as a “hybrid passive control system” that consists of two or more different kinds of passive elements combined into a single device or system. The VE-BRB investigated in this study consists of a rate-independent hysteretic component (BRB) and several rate-dependent damping components (viscoelastic, VE, layers) in innovative configuration to provide phased behavior, additional damping, and improved performance.

The construction principle of the VE-BRB is that several VE layers are assembled into conventional BRB with flat-plate steel core in parallel, and the global construction scheme of the VE-BRB is shown in Fig. 7(a). The BRB part is mainly composed of flat-plate mild steel core,

concrete filled steel tube and de-bonding material layer eliminating friction between the core and the concrete. The BRB part is shown in Fig. 7(b). The VE layer part mainly consists of fixation steel plate, VE material (high damping rubber) layer, and shear steel plates which constitute the sandwich construction form as can be seen in Fig. 7(c). The shear steel plate and high damping rubber layer may be extruded by the steel core which may buckle when it carries axial compression force. To provide reliable lateral support for the core and protect the high damping rubber from serious extension, two spacers are welded near two VE layers' ends on the steel plates respectively, which are shown in Fig. 7.

The theoretical advantages of VE-BRB are described as follows: 1) Suppressing buckling of conventional braces, symmetrical hysteresis loops in tension and compression and developing to the full capacity of strength, ductility, and energy-dissipation; 2) Having the potential to protect the structures over a broad range of earthquake magnitudes (displacement amplitudes), especially to reduce the construction cost based on structural design under minor earthquake and meet the comfort requirements under minor vibrations; 3) Stiffness and energy-dissipation capacity of VE-BRB are stronger than conventional BRB and VE damper due to the combination of both components to work together; and 4) Fatigue capacity of high damping rubber is greater than low yield point steel, and therefore, even if the steel core is snapped under cyclic loading, the VE layers are still able to work normally and, thus, provide multiple security assurance for structures.

VE-BRB's working state can be divided into three phases. Before yielding of the steel core, the shearing strains in the VE material provide sufficient damping to mitigate minor vibrations. After yielding of the steel core, the steel's hysteretic deformations provide supplemental dissipation capacity for greater vibrations. After possible rupture of the steel core under severe excitation, the VE layers can still resist forces and dissipate energy. The phased behavior of VE-BRB can reduce structural responses during minor and major earthquakes because of its significant dissipation capacity. In addition, VE-BRB can be designed as part of a seismic protection system to meet multiple performance-based objectives.

4. Mechanical analysis for VE-BRB

4.1 Mechanical model for the steel core and VE layers

To analyze and calculate the mechanical behavior of the steel core conveniently without too much deviation, the bilinear hysteresis model (Pratap *et al.* 1994) is chosen to simulate the steel core as illustrated in Fig. 8.

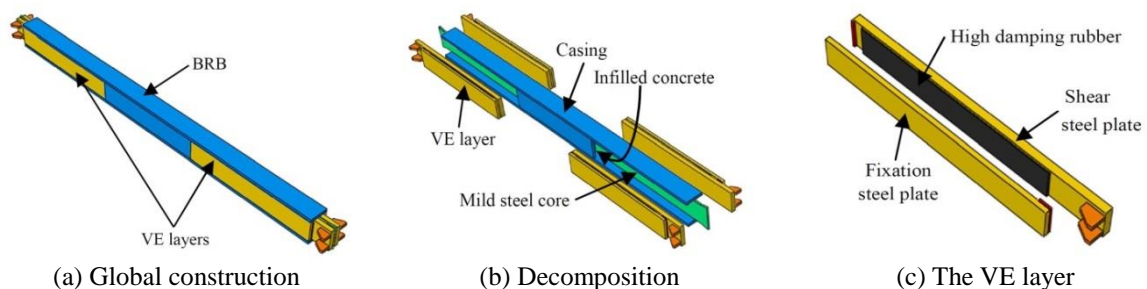


Fig. 7 Major components of a VE-BRB

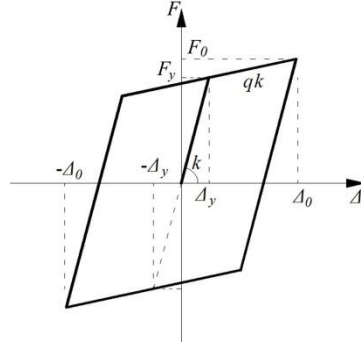


Fig. 8 Bilinear hysteresis model of the steel core

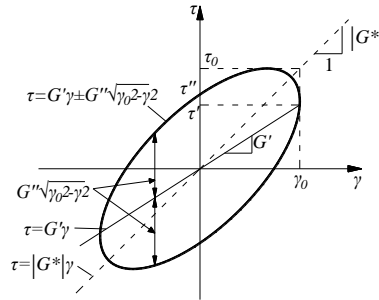


Fig. 9 Stress-strain curve of VEM

Force-displacement relationship of bilinear hysteresis model for elastic stage is

$$F = k\Delta \quad (1)$$

while for plastic stage is

$$F = F_y + qk\left(\Delta - \frac{F_y}{k}\right) = qk\Delta + (1-q)F_y \quad (2)$$

where k = initial stiffness of steel core; F_y = yield force of steel core; q = enhancement factor, which range from 2% to 5%.

Energy-dissipation per cycle of the steel core is expressed as

$$W_c = 4(F_y\Delta_0 - F_0\Delta_y) \quad (3)$$

The stress-strain constitutive model of VE layer is presented in Fig. 9 (Chang *et al.* 1993).

The equivalent shearing storage G' and equivalent shearing loss modulus G'' can be obtained from VE material's performance test. These two parameters are independent of the geometry size of VE layer. The equivalent stiffness k_{eq} , and energy-dissipation per cycle W_d of VE material can be obtained as

$$k_{eq} = \frac{G'A_v}{h} \tag{4}$$

$$W_d = \pi G'' A_v \gamma_0^2 h \tag{5}$$

where A_v = shearing area of VE layer; h = thickness of VE layer; γ_0 = shearing strain of VE layer.

4.2 Global force analysis and mechanical model for VE-BRB

The steel tube of VE-BRB, which is a compression-bending member, carries not only bending moment and end shear but also the axial force transferred from VE layers at both brace ends. Hence, the bearing mode of VE-BRB is different from the conventional BRB. The schematic global mechanical model of the VE-BRB is presented in Fig. 10.

The VE layers at the same side work in series while the steel core and VE layers work in parallel. Deformation and energy-dissipation of steel tube of VE-BRB can be ignored. The global mechanical and energy-dissipation model of VE-BRB is shown in Fig. 11.

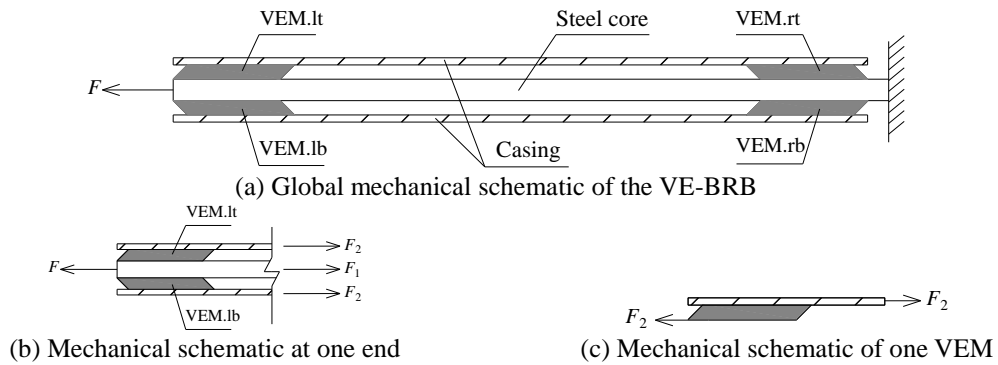


Fig. 10 Global mechanical schematic of the VE-BRB
 (lt = left-top; rt = right-top; lb = left-bottom; rb = right-bottom;
 F_1 = internal force of the steel core; F_2 = shearing force of one VE layer)

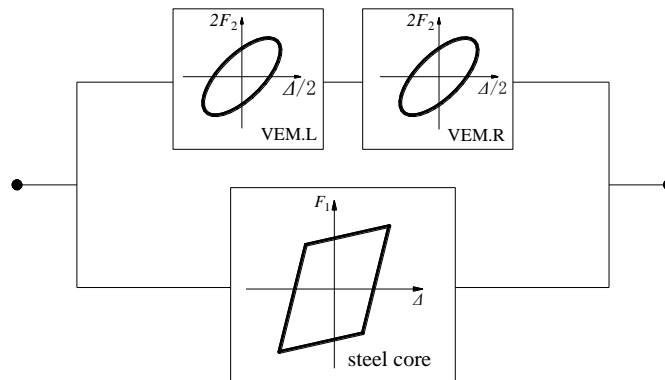


Fig. 11 Force mechanism of the VE-BRB

Both the stiffness and energy-dissipation capacity of VE-BRB are larger than conventional BRB under the same global axial deformation due to the contribution of VE layers. Compared to BRB, the proportion of increased internal force of VE-BRB theoretically is given by

$$\Delta_F = \frac{2F_2}{F_1} \times 100\% \quad (6)$$

The proportion of increased energy-dissipation per cycle is given by

$$\Delta_w = \frac{4W_d}{W_c} \times 100\% \quad (7)$$

4.3 Design considerations

The design method of steel core, connection portion and stability of brace ends of VE-BRB are all the same as conventional BRB. Considering the additional axial force of steel tube of VE-BRB, a moment amplification factor method of steel tube proposed by Zhao *et al.* (2013) can be adopted to check the stability of VE-BRB. The checking formula for conventional BRB can be given by

$$\varphi \left[\omega(\beta-1) \frac{P_{yc}}{P_{yb}} + \alpha_b \frac{M_{b,tr}}{M_{yb}} \right] = \varphi \left[\omega(\beta-1) \frac{P_{yc}}{P_{yb}} + \alpha_b \frac{Pe_{b,tr}}{M_{yb}} \right] < 1 \quad (8)$$

where φ = the stable capacity adjustment coefficient (not less than 1.1); ω = the strain hardening factor; β = the compression strength adjustment factor; P = the yield force of BRB based on material property test; P_{yc} = the yield force of the steel core; P_{yb} = the yield force of the casing; α_b = the moment amplification factor; $e_{b,tr}$ = the triggering eccentricity; M_{yb} = the yield moment of the casing; $\omega(\beta-1)P_{yc}$ = the largest axial force the casing of BRB may carry; when designing VE-BRB, this term should be added with the additional shear forces provided by VE layers, namely $\omega(\beta-1)P_{yc}+2F_2$.

5. Performance tests

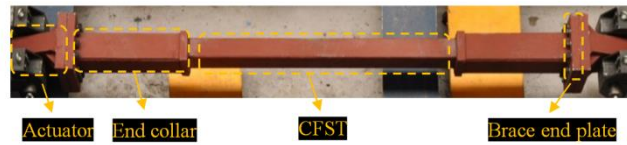
5.1 Specimens description

Two specimens were tested, one VE-BRB specimen and one BRB specimen for performance comparison. The restraining system of the BRB specimen consists of concrete filled steel tube. Both specimens' ends are welded to brace end-plates which are spliced with pinned connector end-plates by split bolts. At the end, the connecting joint is connected to the actuator by pins at each end. It can be found from previous studies (Zhao *et al.* 2012) that this hinge connection easily results in local compression-bending failure at the unconstrained portion of steel core, so an end collar, which was fabricated by welding two short steel angles together to form a tube-shaped cross section, was welded to the end plate. Such configuration was similar to that of the BRB developed by Star Seismic Company (Merritt *et al.* 2003) and that of the inner stiffening tube developed by Kawasaki Steel Corporation (Shimizu *et al.* 2001). Therefore, the brace end configuration adopted for these two specimens is representative of the current state-of-the-practice pin-connected BRBs. The design dimensions and parameters for both specimens are summarized in Table 1. The VE

layer thickness is 10 mm. The pictures about construction detail and connection of braces are shown in Fig. 12; the construction detail of VE-BRB and BRB specimens are shown in Figs. 13 and 14, respectively; the different parts of steel core can be seen in Fig. 15.

Table 1 Main design dimensions and parameters of specimens

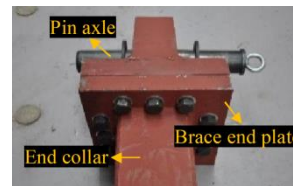
Specimen	Q235 flat-plate steel core				Q345 casing		Stiffness ratio	Brace length/mm
	Section size/mm	Yielding length/mm	Total length/mm	Plate thickness/mm	profile size/mm	Length/mm		
BRB	14×158	2980	3130	20	140×180	2900	6.30	3790
VE-BRB	14×158	2680	3210	20	140×180	2800	8.06	3710



(a) Construction detail of each part of brace



(b) Brace ends construction detail



(c) Pinned connector

Fig. 12 Construction detail and connection of braces

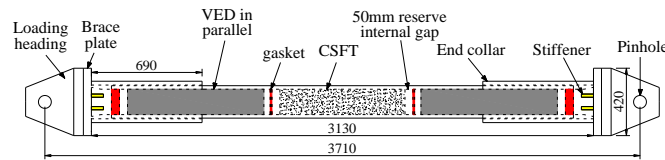


Fig. 13 Construction detail of VE-BRB

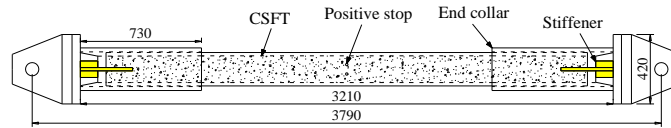


Fig. 14 Construction detail of BRB

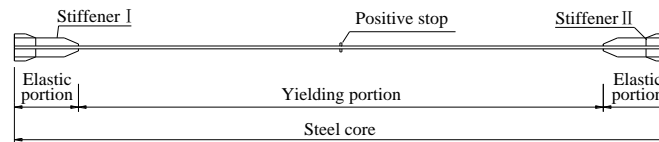


Fig. 15 Different parts of steel core

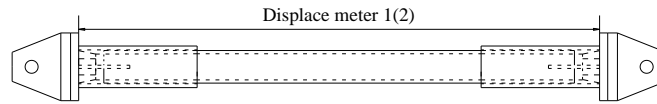


Fig. 16 Location of displacement meters

5.2 Loading and measurement

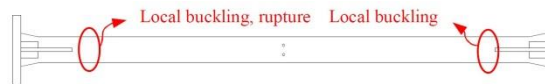
Since the performance of VE material is velocity-dependent, cyclic loading tests need to be conducted. The specimens were subjected to harmonic, displacement-controlled repeated loading, whose frequency was 0.3 Hz and the maximum displacements u_0 were 4mm (keeping the steel core elastic), $L/300$, $L/200$, $L/150$ and $L/100$ (L = total length of brace), respectively, under various loading cases. A total of 30 cycles were applied during the last loading case ($u_0 = L/100$) and 3 cycles were applied during other loading cases.

The axial forces of the specimens were recorded by the actuator. Two string displacement meters, labeled as 1 and 2, were mounted between two end plates of the brace, as shown in Fig. 16, to measure the axial deformation of the specimens. The average of those two recorded displacements was regarded as the global axial deformation of the brace to eliminate the deviation of somewhat gap existing in the pinned connection, elastic deformation of the core connection portion and global flexural deformation of the brace.

5.3 Experimental phenomena and failure modes

5.3.1 BRB

The loading of the BRB specimen was completed smoothly. Under compression, due to the suppression of end collars, the unconstrained portion of the steel core had not ever occurred local bulking, and the brace ends rotated around the pin connector slightly. As the loading process continued, the brace strain and axial force increased consequently. The brace specimen finally experienced rupture and failed to carry load after the 25th cycle during the last loading case ($u_0 = L/100$). It must be noted that at one of the ends of the steel core occurred local buckling and rupture, and at the other one also occurred slightly local buckling; these failure modes were clearly observed after cutting off the casing of the BRB specimen as shown in Fig. 17.



(a) Damage distribution of the core



(b) Local buckling and rupture at one end



(c) Local buckling at another end

Fig. 17 Failure mode of the BRB

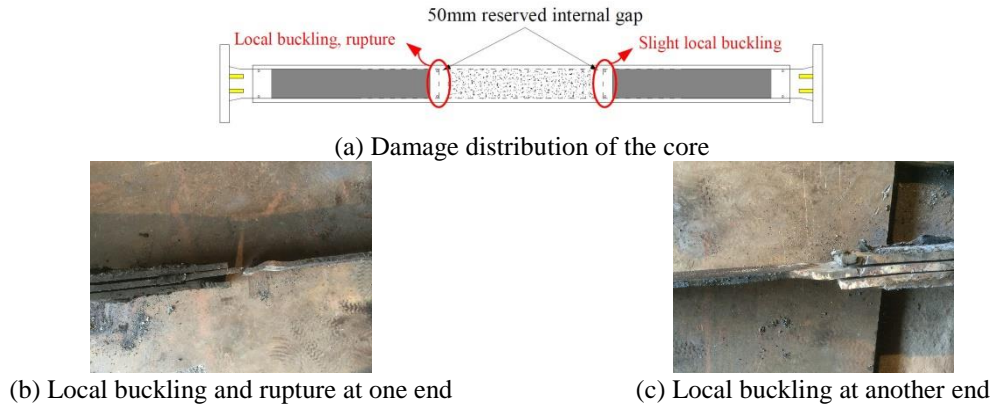


Fig. 18 Failure mode of the VE-BRB

5.3.2 VE-BRB

During the first loading case ($u_0 = 4$ mm) of the VE-BRB specimen, the loading process was smooth and testing responses were similar to those of the BRB specimen. During the second loading case ($u_0 = L/300$), “stress reaction” occurred in the loading system and the loading was not controlled. The VE-BRB specimen was subjected to serious shock wave, which was not expected, and reached a maximum tension force of 1024 kN and a maximum compression force of 876 kN, close values to the theoretical limit capacity of the brace. Therefore, stiffness degradation was found when the second loading case was re-conducted (as shown from the hysteresis loops in Fig. 19(b)). However, the brace specimen could still carry larger forces, so the subsequent loading process went on. The brace specimen experimented ruptured after the 4th cycle of the last loading case ($u_0 = L/100$). But the testing facility’s data collecting system showed that the brace specimen could still carry symmetric axial forces, denoting that VE layers still worked normally.

Considering the construction details, two 50 mm-gaps were reserved between the shearing steel plates of the VE layers and the concrete infill. It can be found that the local buckling and rupture were near of these two gaps, after cutting off the casing of the VE-BRB specimen. The part of the steel core which was constrained by the shearing steel plates and the infilled concrete was flat and smooth, and obvious high-order buckling mode did not occur. This means that the inner construction detail of the VE-BRB specimen is adequate and the VE layers were able to generate shearing strain and dissipate energy, and would not be extruded seriously by large buckling deformation of the steel core. The failure mode of the VE-BRB specimen is shown as Fig. 18. Hence, the inner full-length constraint of steel core by the casing is very important, and the reserved gaps should be minimized to enhance the brace’s capacity.

5.4 Hysteretic responses

The measured hysteresis loops of two brace specimens are shown in Fig. 19. The positive and negative signs denote tension and compression, respectively. The degradation of loading-bearing capacity is marked with shaded triangle in Fig. 19.

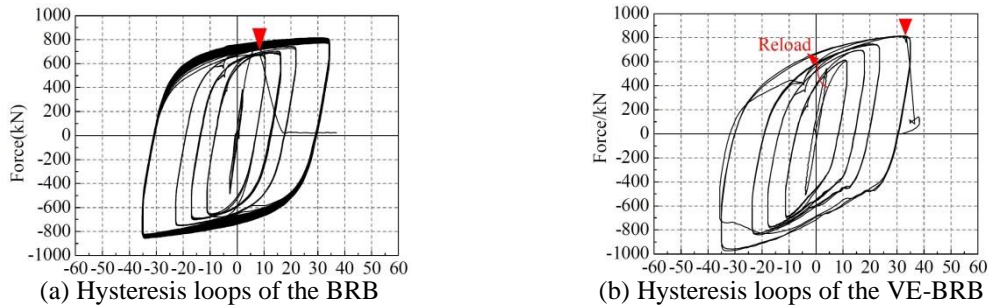


Fig. 19 Experimental hysteresis loops of specimens

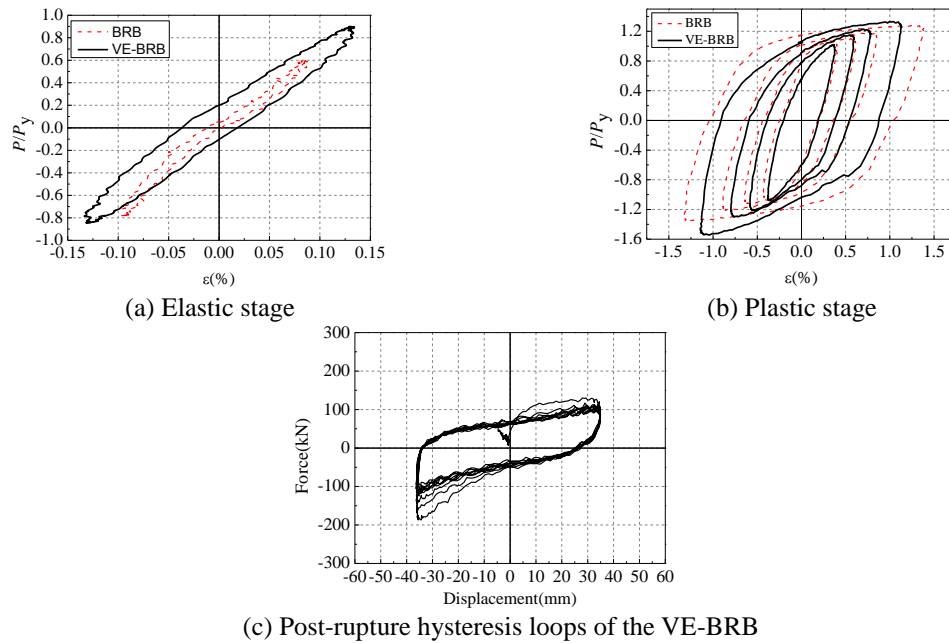


Fig. 20 Comparison of the hysteretic loops between BRB and VE-BRB

The comparison of the normalized hysteresis loops between BRB and VE-BRB is plotted in Figs. 20(a) and 20(b), in which P/P_y means the normalized axial force ($P =$ axial force; $P_y =$ the axial yield force) and ϵ means axial strain of the braces. For clear comparison, only the second cycle hysteresis curves in each loading case which is more stable are plotted here.

It is shown that the hysteresis loops of the BRB are very small at elastic stage, indicating rarely dissipated energy. On the other hand, at elastic stage, the hysteresis loops of the VE-BRB are larger indicating that the VE-BRB can dissipate energy by VE layers. Compared to the BRB, the VE-BRB possesses similar areas of the hysteresis loops, while greater stiffness under each loading case. From the above mentioned experimental phenomenon and the plump hysteresis loops shown in the Fig. 20(c), we could know that after rupture of the core, the BRB stopped working while the VE-BRB could still carry forces and dissipate energy. However, the steel core can still bear small

force during compression even after rupture, resulting in a slight hardening of the hysteresis loops during compression. Therefore, the results validate VE-BRB's multi-phased nature and dissipation capacity, and indicate that VE-BRB not only contains multiple energy-dissipation mechanism, but also provides multiple security assurance for structures.

5.5 Seismic performance evaluation

5.5.1 Compression strength adjustment factor β

Due to the friction existing in the brace, the maximum compression force is larger than the maximum tension force. This characteristic of the brace's axial forces, P_{\max}^i , can be denoted by compression strength adjustment factor β : $\beta = \max(P_{c,\max}^i / P_{t,\max}^i)$, where $P_{c,\max}^i$ and $P_{t,\max}^i$ mean the maximum compression and tension force of the i^{th} cycle for each loading case, respectively.

Compression strength adjustment factors of both BRB and VE-BRB specimens meet the requirement of the "Seismic Provisions for Structural Steel Buildings" (ANSI/AISC 341-10 2010) which indicated that this factor shall be less than 1.3. It means that the construction design of the de-bonding material is reasonable.

5.5.2 Energy dissipation capacity

The equivalent damping ratio of energy-dissipation device is given by

$$\zeta = \frac{E_D}{4\pi E_s} \quad (9)$$

where E_D = dissipated energy; E_s = strain energy.

The larger value of ζ the greater the capacity of energy-dissipation is. The dissipated energy E_D and the equivalent damping ratio ζ can be calculated using the second hysteresis loops from each loading case, which are summarized in Table 2.

The energy-dissipation capacity of the VE-BRB is better than BRB at elastic stage and post-rupture stage. And the great capacity of energy dissipation of VE-BRB in all stages is verified.

During the plastic stage of each loading cases, the hysteresis loop's area of the VE-BRB is slightly smaller than that of the BRB. The main reason may be as follows: 1) The core's yield length of the BRB is about 0.9 times of that of VE-BRB, so the steel core's yield strain and stress is greater than that of VE-BRB under the same displacement; and 2) The shock wave produced by "stress reaction" in the testing facility may decrease the material property of the steel core of VE-BRB.

Table 2 The dissipated energy ED and equivalent damping ratios ζ

Specimen	Index	Elastic stage	$u_0 = L/300$	$u_0 = L/200$	$u_0 = L/150$	$u_0 = L/100$	Post-rupture
BRB	E_D / J	310	17101	31749	47425	86132	/
	$\zeta / \%$	1.3	43.1	46.5	47.4	49.3	/
VE-BRB	E_D / J	1274	15549	31896	47176	82902	7344
	$\zeta / \%$	10.3	34.3	40.3	42.3	43.7	30.3

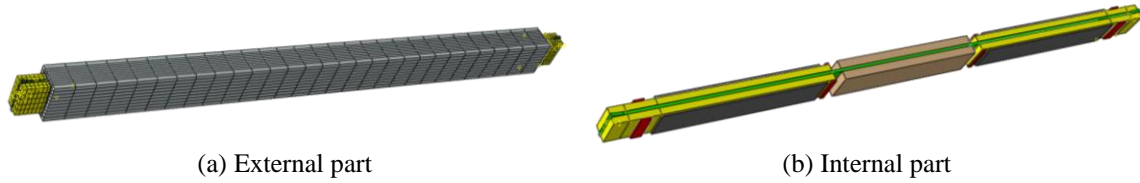


Fig. 21 Finite element 3D model of the VE-BRB

5.5.3 Cumulative plastic deformation

The plastic deformation and fatigue performance of the specimens under cyclic loading can be reflected by the cumulative plastic deformation (CPD) which can be obtained as (Zhao 2012)

$$\text{CPD} = \sum_i^n \left[2 \left(\left| d_{\max}^i \right| + \left| d_{\min}^i \right| \right) / d_y - 4 \right] \quad (10)$$

where d_{\max}^i (d_{\min}^i) and d_y represent the maximum (minimum) displacement and yielding displacement of the i^{th} cycle, respectively, during the whole test. The calculated CPD of VE-BRB is 889, while that of BRB is 202. The CPDs achieved by both specimens were greater than 200 required by “*Seismic Provisions for Structural Steel Buildings*” (ANSI/AISC 341-10 2010) for brace’s uniaxial test.

6. Finite element analysis

6.1 Development of FE models

The FE modeling for the BRB and VE-BRB specimens was performed using the ABAQUS software, and the FE model of the VE-BRB specimen is shown as Fig. 21. To simplify the analysis, the end collar is not considered in the modeling, and instead its constraint effect on the unconstrained portion of the steel core is considered by setting a rotation constraint boundary at the corresponding place. VE material is modeled by hybrid linear isoparametric solid elements (C3D8H), and the other materials are modeled by reduced-integration linear isoparametric solid elements (C3D8R) with hourglass control. In order to consider the velocity-dependence of the VE material, the implicit standard/dynamic method in ABAQUS is adopted for the analysis.

6.2 Material constitutive models and their verification

6.2.1 The combined hardening model for low yield point steel

Under cyclic loading, the simulation results of low yield point steel would be more accurate by using combined hardening constitutive model (Andersson *et al.* 2010). The definition of the constitutive model for steel core material, Q235 steel, is completed by using the ABAQUS “cycle hardening” material property module; the parameters of the combined hardening model are shown in Table 3.

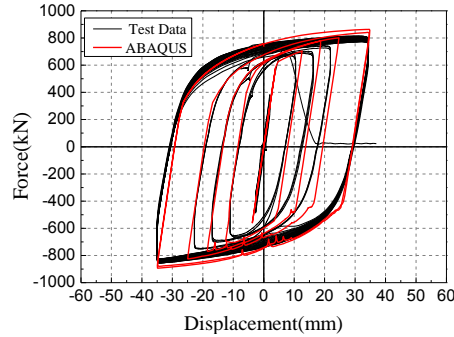


Fig. 22 FE simulation hysteresis loop of the BRB

Table 3 Parameters of the combined hardening model for Q235

Parameter	σ_0 / MPa	C_1 / MPa	γ_1	C_2 / MPa	γ_2	C_3 / MPa	γ_3	Q_∞ / MPa	b
Value	280	16061	151	315	158	64	3.5	100	1

The finite element simulation of the BRB specimen, which employs the constitutive parameters of Q235 steel in Table 3, is shown and compared with test data in Fig. 22. The results indicate that both experimental and FE simulation hysteresis loops agree well and, thus, the constitutive model and parameters are verified.

6.2.2 Constitutive hyper-viscoelastic model for VE material

In ABAQUS software, VE material is simulated by applying the hyper-viscoelastic model (Andersson *et al.* 2010) (generalized Maxwell model), which includes not only the hyperelastic constitutive model, but also the viscoelastic constitutive model. In the hyper-viscoelastic model, velocity-dependency of VE material can be considered, while its amplitude-dependency is considered through using different constitutive parameters under various strains.

The hyper-viscoelastic constitutive characteristics can be described by Mooney-Rivlin model, and the model's parameters are as follows: $C_{01}=1.647 \times 10^3$, $C_{10}=66.896 \times 10^{-3}$ and $D_1=8.755 \times 10^{-3}$. The fitting quasi-static shearing modulus is 0.137MPa, which is close to the value obtained from the material's performance test. The real phase and the imaginary phase of the complex shearing modulus are given by

$$\omega \operatorname{Re}(g^*) = \frac{G''}{G_\infty} \quad (11)$$

$$\omega \operatorname{Im}(g^*) = 1 - \frac{G'}{G_\infty} \quad (12)$$

where G' = shearing storage modulus; G'' = shearing loss modulus.

The VE material parameters under various strains converted from G' and G'' which can be obtained from the material's performance test as listed in Table 4.

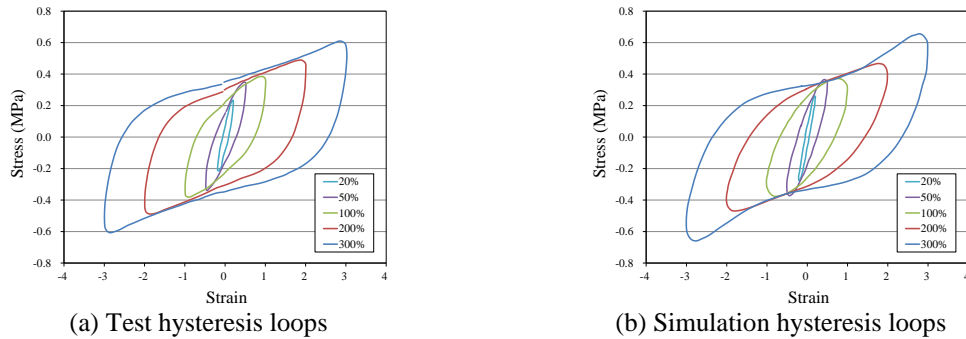


Fig. 23 The test and simulation hysteresis loops of VE material

Table 4 The VE material parameters under various strains

Shearing strain	$\omega Re(g^*)$			$\omega Im(g^*)$		
	0.1Hz	0.3Hz	1.0Hz	0.1Hz	0.3Hz	1.0Hz
0.20	2.628	3.139	3.504	-6.080	-7.613	-9.949
0.65	1.825	2.263	2.555	-2.358	-3.015	-4.036
0.95	1.533	1.825	2.190	-1.336	-1.701	-2.504
1.2	1.387	1.606	1.898	-0.898	-1.190	-1.847
1.75	1.095	1.314	1.533	-0.460	-0.679	-0.971

The test and simulation hysteresis loops of VE material are shown in Figs. 23(a) and 23(b). Comparing the results, the constitutive parameters and modeling method are correct and reasonable.

6.3 Simulation results

High-order buckling modes and stress distribution of the BRB and the VE-BRB are shown in Figs. 24 (a) and 24(b) respectively.

The simulating hysteresis loops of steel core are compared with those of the whole VE-BRB in Fig. 25. The lack of contribution from VE layers makes the axial force and the energy dissipation of the steel core smaller than the entire VE-BRB.

The comparison of hysteresis loops of VE-BRB between simulation and test is shown in Fig. 26. Because friction was not considered in the ABAQUS model, the tension forces are roughly equal to the compression forces. In addition, the areas of the hysteresis loops of VE-BRB in test are relatively smaller than those in the simulation due to damages and performance degradation of the steel core caused by “stress reaction” in the testing facility.

The comparison of hysteresis loops of VE layers only between simulation and test is shown in Fig. 27. The result indicates that the modeling results agree well with the test results, and verifies the energy dissipation property of the VE layers in VE-BRB, especially after the failure of the steel core.

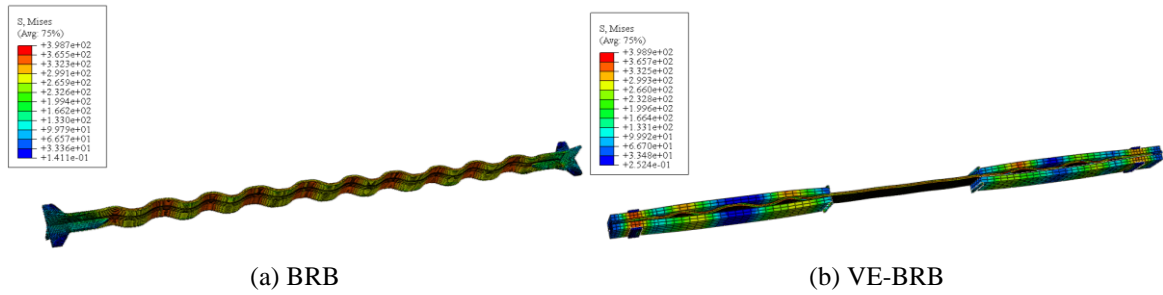


Fig. 24 Higher buckling mode and stress distribution

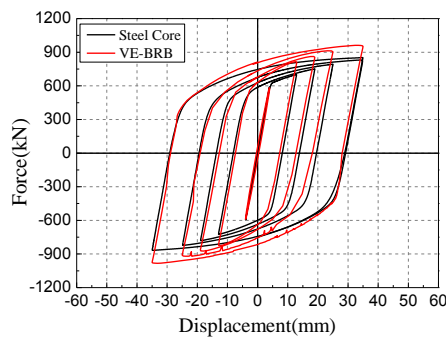


Fig. 25 Comparison of the simulating hysteresis loops between steel core and the entire VE-BRB

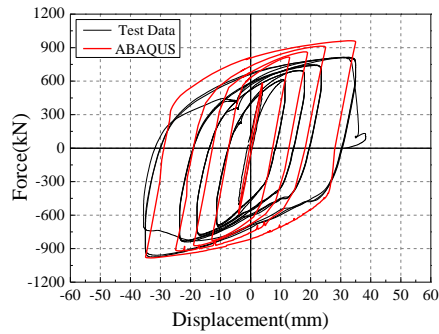


Fig. 26 Comparison of hysteresis loops of VE-BRB between simulation and test

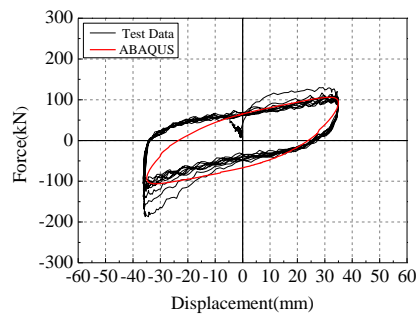


Fig. 27 Comparison of hysteresis loops of VE layers after the failure of the steel core

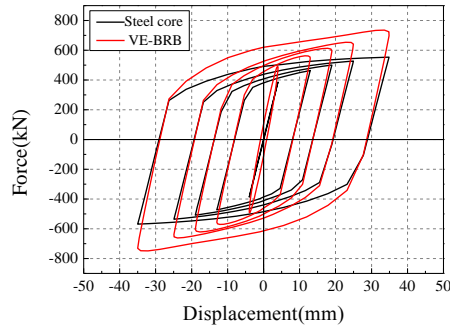


Fig. 28 Hysteresis loops of the optimized VE-BRB

6.4 Optimization of VE-BRB

From the Eq. (5), the conclusion that can be drawn is that the energy dissipation capacity of the VE layer is stronger when the shearing area A_v is larger and thickness h is smaller at the same displacement amplitude u_0 . Based on the principle that the steel core works in parallel with the VE layers, it is known that the performance of the VE-BRB will be much better and the proportion of energy dissipation assumed by VE layers gets larger.

Based on the above theory, the profile of the steel core of the original VE-BRB can be reduced from 14 mm×158 mm to 12 mm×120 mm, and the thickness of VE layers can be reduced from 10 mm to 5 mm, as other conditions are invariant. With the same FEA method, hysteresis loops of the optimized VE-BRB are shown in Fig. 28. The result indicates that proportions of increased axial force and energy-dissipation provided by VE layers have been improved.

7. Seismic analysis of steel braced frames

To provide verification of the benefits of VE-BRB for seismic protection of structures, and compare its seismic performance with BRB. This was done by performing a time history analysis of a multistory frame structure with VE-BRBs and BRBs, respectively.

7.1 Basic information of the frame structure

The prototype building for this analysis is a 6-story steel braced moment resisting frame structure from a reference study (Guo 2007), whose structural plane dimensions are 31.2 m×23.4 m. The plan and elevation of the frame structure are shown in Fig. 29, and the sizes of columns and beams are summarized in Table 5. The whole structure uses Q235 steel. Because the structural plane layout is basically symmetric, the effect of structural torsion can be ignored. The double-lines shown in Fig. 29(a) denote single diagonal brace arranged for each place there. To reduce structural torsion effect, the frames adopt symmetric single braces arrangement as illustrated in Fig. 29(b). The standard value of floor live load is 2.5 kN/m², and dead load (including the self-weight of floor, secondary beam, filler wall and so on) is 6.0 kN/m².

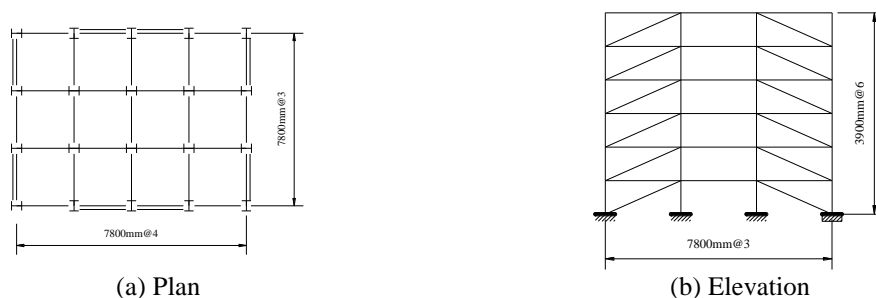


Fig. 29 Plan and elevation of the frame structure

Table 5 Profiles of columns and beams

Elements	Profiles
Columns of 1st~3rd story	HW450×450×16×24
Columns of 4th~6th story	HW350×350×12×21
Beams	HW450×300×12×18

7.2 Finite element models

The finite element models for the moment resisting frame structures with BRBs and VE-BRBs are developed in the ABAQUS software. Structural masses and lateral stiffness are simplified to establish a planar frame model, shown in Fig. 30, assuming that the in-plane stiffness of the floor is rigid without consideration about the structure's torsion effect. The FE models of frame with VE-BRB and BRB are shown in Fig. 30.

The connections between the braces and the frames adopt pin connection of MPC. The bottom joints of the frame columns are coupled by kinematic constraint with a reference point that is consolidated. The seismic record is applied to the reference point in the form of acceleration data.

The bilinear kinematic hardening material model is adopted for the steel frame model. The design value of the material's strength f_y is 205MPa; Poisson ratio is 0.3; Young's modulus is 2.06×10^5 MPa; and hardening factor is 2%. Beams and columns of the structure are modeled by B31 elements considering shearing deformation. BRBs are modeled by T3D2 element (Andersson *et al.* 2010), which is truss element bearing only axial loads. VE-BRBs are modeled by T3D2 element combined with one linear spring and one linear dashpot in parallel for considering VE layers, shown as Fig. 31.



Fig. 30 The simplified planar FE models

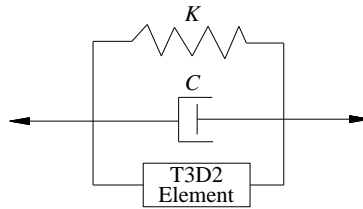


Fig. 31 The composition of VE-BRB element

Table 6 K_{eq} and C_{eq} of the equivalent VE layer

Shear strain	0.1	0.2	0.5	1	2	3
$K_{eq} (\times 10^6 \text{N/m})^*$	102.5	75	38.5	21.5	12	10
$C_{eq} (\times 10^6 \text{N}\cdot\text{s/m})$	4.5	3.85	2.95	2.25	1.55	1.2

* K_{eq} and C_{eq} over other shearing strains can be obtained by linear interpolation

Design parameters of the above mentioned optimized VE-BRB model are adopted here. The cross-section of the steel core is 12 mm×120 mm. Four VE layers can be equivalent to one layer, whose equivalent thickness and shearing area is 2×6 mm and 2×120 mm×2500mm, respectively, according to their series-parallel relationship. For comparison, the cross-section of the steel core of BRB is also 12 mm×120 mm.

The combined hardening constitutive model with the parameters shown in Table 3 is adopted by T3D2 elements for BRB and VE-BRB. The brace's theoretical yield force is 400 kN and length is 8.72 m. Since the natural frequency of the frame is about 1.0 Hz, the equivalent stiffness K_{eq} and the equivalent damping C_{eq} of the equivalent VE layer (simulated by the linear spring and viscous dashpot shown in Fig. 31) under different strains and frequency of 1.0Hz are listed in Table 6. Based on this FEA method, the simulated hysteresis loops are obtained and compared with those of the testing as shown in Fig. 32. It is found that equivalent stiffness and damping of the simulated loops, which are essential parameters for VE material to control structural responses, agree well with those of the testing loops. So the rationality of the FEA method about VE layers is verified.

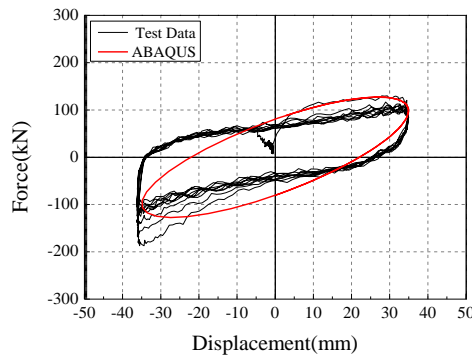


Fig. 32 Hysteresis loop of the equivalent VED

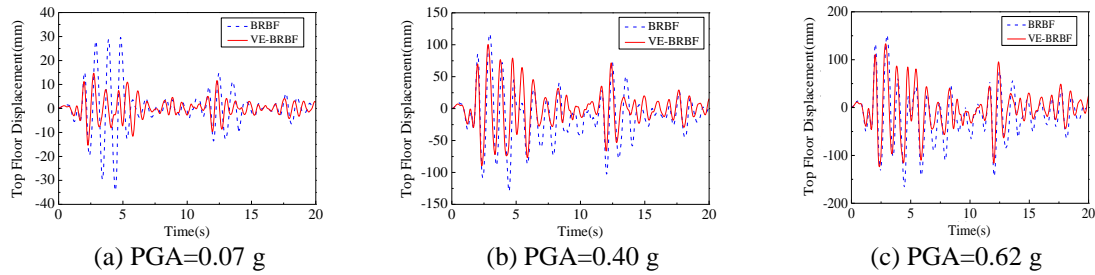


Fig. 33 Roof displacement of the structures (former 20s)

7.3 Time history analysis

The El Centro record was selected and input into the structural model. The braced frame structure is assumed to be constructed in a seismic fortification intensity zone of 8-degree (GB 50011-2010), so the peak ground acceleration (PGA) is 0.07 g, 0.40 g and 0.62 g for minor, moderate and major earthquake, respectively, based on Chinese specification GB 50011-2010.

7.3.1 Roof displacement

The roof displacement of the braced structures under different intensities of the excitation is shown in Fig. 33, in which BRBF and VE-BRBF mean BRB-braced and VE-BRB-braced frame structure, respectively. The figures reveal that the control effect of VE-BRB on the roof displacement is better than that of BRB, especially under minor earthquake. This is because BRBs would not yield and absorb energy under minor earthquake, while VE-BRBs provide additional damping for energy dissipation by VE layers to mitigate the displacement response of the structure effectively.

7.3.2 Base Shear

The base shear of the braced structure under different earthquake levels is shown in Fig. 34. The figures show that the base shear of VE-BRB is slightly smaller than that of BRB when the PGA is small, but it increases quickly and then is slightly greater than the latter one as the PGA increased, which might be caused by the greater stiffness of VE-BRB.

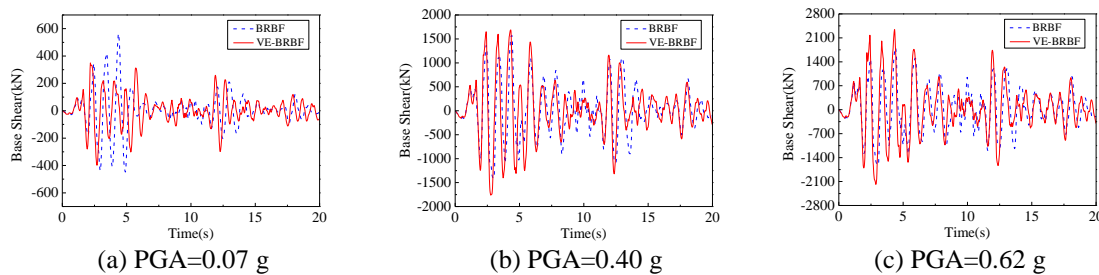


Fig. 34 Base shear of the structures (former 20s)

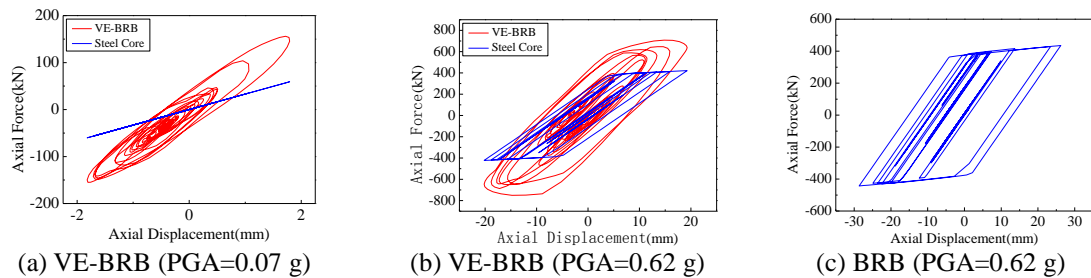


Fig. 35 Hysteresis loops of one brace at the 3rd story

7.3.3 Hysteresis loops of braces

Fig. 35 shows hysteresis loops of one brace (BRB or VE-BRB) at the 3rd story. As shown in Fig. 35(a), the steel core of the VE-BRB is elastic under minor earthquake (steel core of the BRB is in the same situation), so its hysteresis loops show ideal linear elasticity, while the hysteresis loops of the whole brace of the VE-BRB are ellipse-shaped due to the energy dissipation by VE layers. As can be seen in Fig. 35(b), the steel core of the VE-BRB are at plastic stage with parallelogram-shaped hysteresis loops under major earthquake, while the hysteresis loops of the whole brace of the VE-BRB show a shape between ellipse and parallelogram with greater equivalent stiffness and damping. The steel core of the BRB also shows parallelogram-shaped hysteresis loops with smaller maximum axial force than that of VE-BRB under major earthquake as shown in Fig. 35(c). The results indicate that the VE layers can dissipate a large amount of seismic energy for all levels of ground motion, and verify the multi-phased nature and advantages of VE-BRB for structural control and protection.

8. Conclusions

To take advantages of both displacement- and velocity-dependent devices, a new type of hybrid passive control device, named as VE-BRB, consisting of a BRB with high-damping VE layers is proposed and studied. Some beneficial effects from the combination were found, and several conclusions can be reached based on the results of the experimental, theoretical and numerical analysis. The following conclusions can be drawn:

- Cyclic loading tests and their numerical simulations in ABAQUS of VE-BRB and BRB were performed. The results showed that their hysteresis loops were full, stable and symmetric with good fatigue performance, which indicated that the VE-BRB and the BRB specimens have reasonable construction details and great seismic performance.
- The hysteresis loops of VE-BRB were approximately oval-shaped indicating multi-phased nature and good performance. Its equivalent damping ratio equaled to 10% under minor earthquake, which differed from that of the BRB which could not dissipate energy induced by minor earthquake level. Thus, structures are possible to benefit from VE-BRB for a decrease of the construction cost based on structural design under minor earthquake. After failure of the steel core, the VE layers of VE-BRB still worked, with equivalent damping ratio of 30%, providing multiple security structure assurance. The simulation results agreed well with the test results, validating the

finite element analysis method, constitutive models, and the identified parameters for the steel core and VE material.

- The comparative study of the time history analysis on a 6-story frame structure with VE-BRBs and BRBs was conducted. The analytical results verified the advantages of VE-BRBs for seismic protection of structures compared with BRBs. In general, VE-BRB had the potential to provide better control effect on structural displacement and shear in all stages than BRB as expected. The properties of VE-BRB could be adjusted and optimized to meet the design demands through selecting different VE material and metallic yielding material or adjusting their geometric dimensions.

Acknowledgments

The authors are grateful for the financial support received from the National Key Research and Development Program of China (Grant No. 2016YFC0701101) and National Natural Science Foundation of China (Grant No. 51678449). The viscoelastic material provided by the Sumitomo Riko Company in Japan is also acknowledged.

References

- Andersson, B.L., Andersson, P. and Lundwall, J. (2010), *Abaqus/CAE 6.7 User's manual*, Computers Structures.
- ANSI/AISC 341-10 (2010), Seismic provision of structural steel buildings, American Institute of Steel Construction; Chicago, USA.
- Apostolakis, G. and Dargush, G.F. (2010), "Optimal seismic design of moment-resisting steel frames with hysteretic passive devices", *Earthq. Eng. Struct. D.*, **39**(4), 355-376.
- Bazaez, R. and Dusicka, P. (2016), "Cyclic behavior of reinforced concrete bridge bent retrofitted with buckling restrained braces", *Eng. Struct.*, **119**, 34-48.
- Bozkurt, M.B. and Topkaya, C. (2016), "Development of welded overlap core steel encased buckling-restrained braces", *J. Constr. Steel Res.*, **127**, 151-164.
- Chang, K.C., Lai, M.L., Soong, T.T., Hao, D.S. and Yeh, Y.C. (1993), "Seismic behavior and design guidelines for steel frame structures with added viscoelastic dampers", Research Report No. NCEER-93-0009; National Center for Earthquake Engineering Research, Buffalo, NY, USA.
- Chou, C.C., Tsai, W.J. and Chung, P.T. (2016), "Development and validation tests of a dual-core self-centering sandwiched buckling-restrained brace (SC-SBRB) for seismic resistance", *Eng. Struct.*, **121**, 30-41.
- Di Sarno, L. and Manfredi, G. (2012), "Experimental tests on full-scale RC unretrofitted frame and retrofitted with buckling-restrained braces", *Earthq. Eng. Struct. D.*, **41**(2), 315-333.
- El-Bahey, S. and Bruneau, M. (2011), "Buckling restrained braces as structural fuses for the seismic retrofit of reinforced concrete bridge bents", *Eng. Struct.*, **33**(3), 1052-1061.
- GB 50011-2010 (2010), Code for seismic design of buildings, China Architecture Building Press; Beijing, China. (in Chinese).
- Gong, S.M. and Zhou, Y. (2017), "Experimental study and numerical simulation on a new type of viscoelastic damper with strong nonlinear characteristics", *Struct. Control Health.*, **24**, e1897.
- Guneyisi, E.M. (2012), "Seismic reliability of steel moment resisting framed buildings retrofitted with buckling restrained braces", *Earthq. Eng. Struct. D.*, **41**(5), 853-874.
- Guo, Z. (2007), "Seismic performance analysis of steel frame with BRBs. PhD Thesis", Ph.D. Dissertation;

- Harbin Institute of Technology, Harbin, China. (in Chinese).
- Khoo, H.H., Tsai, K.C., Tsai, C.Y., Tsai, C.Y. and Wang, K.J. (2016), "Bidirectional substructure pseudo-dynamic tests and analysis of a full-scale two-story buckling-restrained braced frame", *Earthq. Eng. Struct. D.*, **45**(7), 1085-1107.
- Lee, H.S., Lee, K.B., Hwang, K.R. and Cho, C.S. (2013), "Shake table responses of an RC low-rise building model strengthened with buckling restrained braces at ground story", *Earthq. Struct.*, **5**(6), 703-731.
- Lin, P.C., Tsai, K.C., Chang, C.A., Hsiao, Y.Y. and Wu, A.C. (2016), "Seismic design and testing of buckling-restrained braces with a thin profile", *Earthq. Eng. Struct. D.*, **45**(3), 339-358.
- Mahrenholtz, C., Lin, P.C., Wu, A.C., Tsai, K.C., Hwang, S.J., Lin, R.Y. and Bhayusukma, M.Y. (2015), "Retrofit of reinforced concrete frames with buckling-restrained braces", *Earthq. Eng. Struct. D.*, **44**(1), 59-78.
- Marshall, J.D. and Charney, F.A. (2012). "Seismic Response of Steel Frame Structures with Hybrid Passive Control Systems", *Earthq. Eng. Struct. D.*, **41**(4), 715-733.
- Merritt, S., Uang, C.M. and Benzoni, G. (2003), "Subassemblage testing of star seismic buckling-restrained braces", Research Report No. TR-2003.
- Pratap, R., Mukherjee, S. and Moon, F.C. (1994), "Dynamic behavior of a bilinear hysteretic elasto-plastic oscillator, part I: free oscillations", *J. Sound Vib.*, **172**(3), 321-337.
- Shimizu, T., Fujisawa, K. and Uemura, K. (2001), "Study on hysteresis behavior of double tube steel bracing: part 2 plan of cyclic loading test of double tube steel bracing", *Summaries of Technical Papers of Meeting Architectural Institute of Japan*, Architectural Institute of Japan; Tokyo, Japan.
- Usami, T., Wang, C.L. and Funayama, J. (2012), "Developing high-performance aluminum alloy buckling-restrained braces based on series of low-cycle fatigue tests", *Earthq. Eng. Struct. D.*, **41**(4), 643-661.
- Vargas, R. and Bruneau, M. (2009), "Analytical response and design of buildings with metallic structural fuses I", *J. Struct. Eng.*, **135**(4), 386-393.
- Wei, X.N. and Bruneau, M. (2016), "Case Study on Applications of Structural Fuses in Bridge Bents", *J. Bridge. Eng.*, **21**(7), 1-15.
- Zhang, D.B., Nie, X., Pan, P., Wang, M.Z., Deng, K.L. and Chen, Y.B. (2016), "Experimental study and finite element analysis of a buckling-restrained brace consisting of three steel tubes with slotted holes in the middle tube", *J. Constr. Steel Res.*, **124**, 1-11.
- Zhao, J.X. (2012), "Seismic behavior and stability design methods of buckling restrained braces", Ph.D. Dissertation; Harbin Institute of Technology, Harbin, China. (in Chinese).
- Zhao, J.X., Wu, B. and Ou, J.P. (2011), "A novel type of angle steel buckling-restrained brace: Cyclic behavior and failure mechanism", *Earthq. Eng. Struct. D.*, **40**(10), 1083-1102.
- Zhao, J.X., Wu, B. and Ou, J.P. (2012), "Effect of brace end rotation on the global buckling behavior of pin-connected buckling-restrained braces with end collars", *Eng. Struct.*, **40**(7), 240-253.
- Zhao, J.X., Wu, B. and Ou, J.P. (2013), "Global stability design method of buckling-restrained braces considering end bending moment transfer: Discussion on pinned connections with collars", *Eng. Struct.*, **49**(2), 947-962.
- Zhou, Y. and Chen, P. (2017), "Shaking table tests and numerical studies on the effect of viscous dampers on an isolated RC building by friction pendulum bearings", *Soil Dyn. Earthq. Eng.*, **100**, 330-344.
- Zhou, Y., Lu, X.L., Weng, D.G. and Zhang, R.F. (2012), "A practical design method for reinforced concrete structures with viscous dampers", *Eng. Struct.*, **39**, 187-198.
- Zhou, Y., Zhang, C.Q. and Lu, X.L. (2017), "Seismic performance of a damping outrigger system for tall buildings", *Struct. Control Health.*, **24**, e1864.

